

# Evaluation of deep-space laser communication under different mission scenarios

Abhijit Biswas<sup>\*</sup>, Sabino Piazzolla, Bruce Moision, Douglas Lisman  
Jet Propulsion Laboratory, California Institute of Technology, 4800 Oak Grove Drive,  
Pasadena, CA, USA 91109;

## ABSTRACT

A number of space agencies, including NASA, are considering free-space laser communications as a means for returning higher data-rates from future space missions. In this paper, potential deep-space missions are evaluated to show that with optical communication a 10× increase relative to state-of-the-art telecommunication systems could be achieved. The maximum deep-space distance where ground transmitted laser beacons could assist acquisition and tracking; and operating points where optical communication performance degrades faster than the inverse square distance are also discussed.

**Keywords:** Laser communications; data-rates; data-volumes; mission scenarios

## 1. INTRODUCTION

Free-space laser communication is a promising solution for a 10× increase in space-to-ground data-rates, with respect to Ka-band. Furthermore, the mass and power required is comparable to that used by state-of-the-art high-rate space telecommunication systems. Successful optical link demonstrations utilizing near-Earth spacecraft<sup>1</sup>, have spurred the development of operational optical communication systems for Low-Earth-orbiting (LEO) and geostationary orbiting (GEO) missions<sup>2</sup>. The upcoming Lunar Laser Communication Demonstration<sup>3</sup> (LLCD) will validate bi-directional space-to-ground optical links over Earth-Moon distances. Missions beyond the Moon involve a progression of increasing round-trip-light-times (RTL<sup>T</sup>'s): 10's of second's (Earth-Sun Lagrange points); minutes (Mars); hours (Saturn and beyond). With incremental technology advances the development of operational optical communications to cover these ranges will no doubt follow. In this paper we present analysis and discussions of the emerging optical communication capability to meet projected future mission needs.

In 2010 NASA sponsored a study called Deep-space Optical Terminals<sup>4</sup> (DOT) to develop a conceptual system design, targeting a 10× increase in data-rate over the Mars Reconnaissance Orbiter (MRO) Ka-band telecommunication system. The DOT system conceptual design comprised of flight and ground terminals has been described in detail<sup>5,6,7</sup>. In this paper we utilize appropriately scaled versions of this system design to address potential (i) Mars science orbiters in Section 2, (ii) outer-planet orbiters in Section 3 and (iii) heliophysics and astrophysics missions at Earth-Sun Lagrange point (L1 & L2) in Section 4. The paper is concluded in Section 5.

## 2. MARS MISSIONS

### 2.1 Reference Optical Communication Architecture

Future Mars mission science, especially high definition imaging, could benefit from optical communication data-rates. Figure 1 provides an architectural view of a ground-based network of optical receivers and transmitters servicing a Mars orbiter. The 22 cm diameter DOT flight laser terminal (FLT) transmitting 4-W of average optical power at 1550 nm is on-board the host spacecraft. M-ary pulse-position modulation (PPM) laser signals (M=16, 32, 64 and 128) with minimum slot widths of 0.5 ns received by photon-counting receivers at the focal plane of 12 m ground telescopes is presumed. The ground-based network assumed is comprised of four receiving stations located at Goldstone (GS), CA,

---

<sup>\*</sup> abiswas@jpl.nasa.gov; phone (818)-354-2415; fax (818)-393-6142

Teide (T), Canary Islands, Alice Springs (AS), Australia and La Silla (LS), Chile. As elaborated later in Section 2, a combination of northern and southern hemisphere sites optimizes mission coverage and data-return. Ground sites where international space agencies either have optical assets or where it would be feasible to deploy ground stations were chosen for our analysis purposes only. Actual sites for potential future optical ground networks would be chosen through site selection studies that are pending. Earth transmitted laser beacon (dashed lines in Fig. 1)) assisted acquisition and tracking by the flight terminal is presumed. Consequently each ground node would have a ground laser transmitter (GLT) and ground laser receiver (GLR) as shown. The GLT and GLR would not necessarily have to be co-located but their angular separation as viewed from space must be compatible the FLT field-of-view (FOV), the point-ahead angle and the desired contact time.

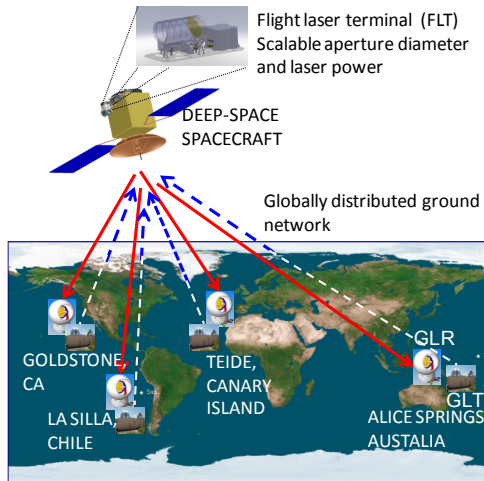


Figure 1. Architectural concept for servicing future space missions is shown with a ground network of four globally distributed ground stations. Each ground station must transmit a laser beacon (blue line) and receive downlink (red line)

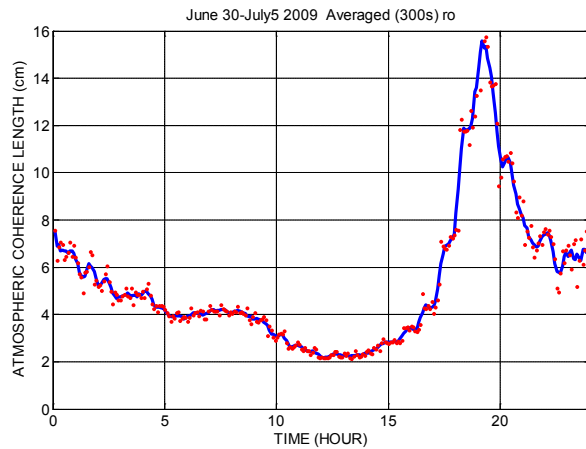


Figure 2. Daily variation of the atmospheric coherence length (red dots) at Goldstone determined using a ground scintillometer with the blue line representing an interpolation of the measurements. The atmospheric coherence length is referenced to an optical wavelength of 500nm at local zenith.

## 2.2 Data Rate Estimation

Downlink data rates were generated using the JPL Deep Space Optical Link (DeSOL) tool that is a MATLAB graphical user interface (GUI) based script capable of computing either a point design or data-rates as a function of varying link parameters during the course of a mission. First, fixed mission link parameters, such as, laser power, transmit/receive terminal diameter's, system efficiency and signaling parameters were entered into the GUI. Next an input file was created, listing time-stamped range, observation zenith angle, Sun-Earth-Probe (SEP) angle, atmospheric-transmittance at local zenith, sky radiance, atmospheric-coherence-length at 500 nm at zenith and sun zenith angle. An output file with time-stamped data-rates was generated.

Preliminary atmospheric characterization measurements<sup>8</sup> for GS, which is the JPL/NASA Deep Space Network (DSN) station were available. These measurements have shown favorable comparison to simulations using the radiative transfer program MODTRAN. Its desert location is characterized by scarce vegetation with dust being the main aerosol component, and dust concentration dependent on local wind speed. The worst case transmittance and daytime sky radiance representing 90% of the cumulative density function (CDF) corresponded to wind speeds of 8.8 m/s. For clear air turbulence at GS, the daily cycle of the atmospheric coherence length (or  $r_0$ ) derived using ground scintillometer measurements was synchronized to the time of day as shown in Figure 2.

We conservatively based our assessment of atmospheric conditions for all ground sites on the GS data and models. AS being another desert location is expected to be similar to GS. For LS and T, the geographical and meteorological conditions suggest "better" atmospheric channel conditions therefore GS can serve as a lower bound on performance. The input file described above was generated for each site using "nominal" and "worst" atmospheric conditions corresponding to 50<sup>th</sup> and 90<sup>th</sup> percentile atmospheric transmission and sky radiance. Atmospheric-coherence-length or

turbulence was determined by time of day in accordance with the model shown in Figure 2. Average site availability is discussed in Section 2.4.

### 2.3 Mission and Link Assumptions

The present analysis assumes a generic Mars science orbiter at an altitude of approximately 400 km from the planet surface with an orbital inclination of 75°. The range and sun-angle variation for the period starting July 30, 2018, was determined using the Satellite Orbital Analysis Program (SOAP) and is shown in Figure 3a. Figure 3b presents a pie chart to partition the mission conditions into “Best,” “Nominal,” and “Worst,” slices, with the associated range and sun-angles indicated. For the present analysis the shaded portion of Fig. 3a spanning approximately one year, from July 30,

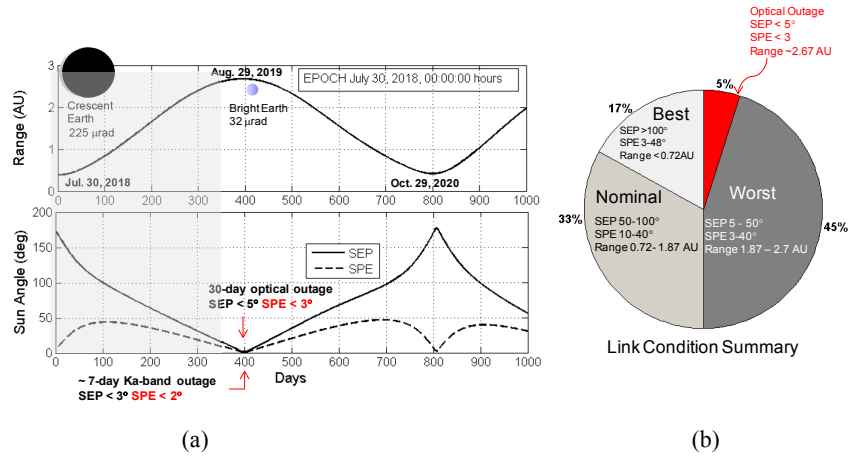


Figure 3. (a) Range and Sun-Earth-Probe (SEP) and Sun-Probe-Earth (SPE) angle variation expected during a typical Mars mission. As the Earth Mars range increases the angular diameter of Earth viewed from the spacecraft decreases but also evolves from a crescent to be fully illuminated bright Earth. (b) A pie chart showing the fraction of time spent at the allocated “Best” “Nominal” and “Worst” link conditions.

2018 to August 28, 2019, was analyzed, since this duration covers all representative mission conditions. Presumed science data produced per sol over the course of the mission is assumed to vary from 1.5 -13.8 gigabytes (GB) with an average of 4 GB or 32 gigabits (Gb). The mission is assumed to carry a solid-state recorder with 20 GB of available memory for storing science data.

Elevation angles with a 20° cut-off from ground sites to the Mars orbiter are shown for two days (July 31, 2018 and August 26, 2019) in Fig. 4a and Fig. 4b. Figure 4a shows low peak elevation angles for GS/T and high peak elevation angles for AS/LS. In Fig. 4b the northern hemisphere sites GS/T display higher peak elevations than the southern hemisphere sites AS/LS. Higher peak elevation angles are indicative of longer contact times. Figure 4c shows the complementary variation in contact time for northern (black points) and southern (light grey points) hemisphere sites, justifying the earlier assertion (Section 2.1) that combined north/south hemisphere nodes on the ground network provide best coverage.

Optical link availability from deep-space is determined by: (i) cloud-free-line-of-sight (CFLOS) duration between ground sites and the spacecraft; (ii) ground-station downtime including conditions, such as, excessive wind or dust storms and humidity. For simplicity, in this study we consider only CFLOS and assume that the stations would be available the remainder of the time. In Table 2 below the first row summarizes the CFLOS availability for the chosen ground sites. This summary is based on satellite data gathered from May 2003 to June 2004 and analyzed under JPL contract<sup>9</sup>. Another noteworthy feature of Figure 4 is the overlap in coverage between 2 and sometimes 3 of the chosen ground sites. For uncorrelated cloud cover at these locations, increased availability relative to a single site could be achieved as indicated in Table 2 with the grey cells corresponding to ground site combinations not encountered or encountered for a negligible fraction of the duration analyzed. Correlated cloud cover is not addressed in our paper.

### 2.4 Data Volume Estimates

Using the procedure outlined in Section 2.2 data-rates achievable with operating points separated by 1-hour intervals were computed. Details on the link analysis used to compute the data-rates are discussed in Ref. 4. Figure 5 shows the

estimated data-volume as a function of time for each site taking into account the contact time (Figure 4c) and availability (first row of Table 2). Filled and clear squares represent nominal and worst atmospheric conditions at intermediate and lowest elevation angles, respectively. The data-volume for an enhanced MRO Ka-band telecom system, with 90% weather availability, is shown (crosses) for comparison with the GS data. The assumed minimum, average and

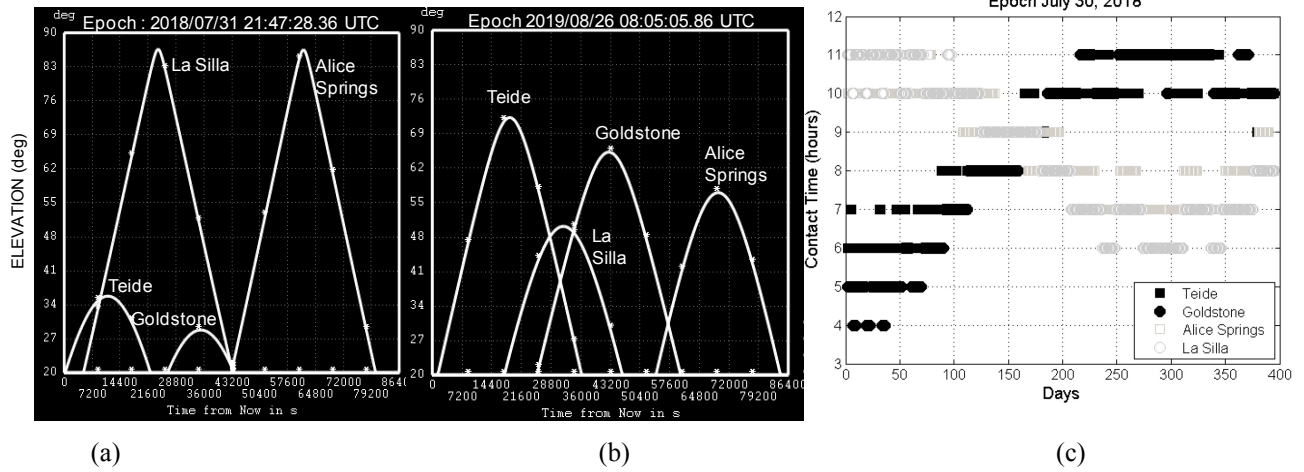


Figure 4. Elevation angle from the different ground sites on (a) July 30, 2018; and (b) August 30, 2019. (c) the variation of contact time to within 1 hour from the Northern hemisphere (GS and T) and Southern hemisphere (AS and LS) sites.

maximum science data intake per sol and the spacecraft data buffer capacity are also shown in Fig. 5a. The integrated data volume achievable for each site, if it were the only ground-station supporting the 389 day mission is annotated on the plots of Fig. 5. Figure 6a plots the time needed to empty the 20 GB spacecraft data buffer as a function of time if any one of the four sites were operating by itself. Beyond 200-300 days (depending on the chosen site) the time to empty 20GB of stored data (see Section 2.3) starts increasing. The rapid rate of increase in this time is noteworthy. Thus, on an average, the spacecraft could be emptied daily until

Table 2 Summary of CFLOS availability of single, two or three ground sites

	Goldstone (GS)	Alice Springs (AS)	Teide (T)	La Silla (LS)
Fractional CFLOS Single Site	0.66	0.58	0.39	0.81
2-site availability with LS	0.94		0.88	
2-site availability with GS		0.86	0.79	
3-Site Availability with GS & T				0.96

mission day 200-300 after which in approximately 50 days the time required to empty the spacecraft buffer may exceed the contact time by a factor  $\sim 5$ . During the last 40 days of the mission this factor could increase to 10. The steep increase in time needed to empty the buffer is somewhat unique to Mars optical links and is discussed further below.

For a four-site ground network the overall contact time would increase to 95%, compared to 35% for any single site. Moreover, the availability would also increase due to overlapping 2- and 3-station line-of-sight as tabulated in Table2. For the orbiter and mission duration analyzed Figure 6b shows a pie-chart of the contact time distribution between the 4-sites with a 5% gap time. The corresponding range of increased integrated data-volume that would result from a 4-site ground network is compared to the data volumes to any single site in the Table of Figure 6c. The large range results from presuming the lowest and highest availability when 2- or 3-sites are simultaneously available.

### 2.5 Optical data rate dependence on signal to noise ratio

In this section we address the steep increase in time required to empty the spacecraft buffer by illustrating that the capacity of the intensity-modulated, direct-detected optical link goes as  $1/R^2$  at high signal-to-noise ratio (SNR), and as

$1/R^4$  at low SNR. SNR refers to the ratio of detected signal and noise power ( $P_r/P_n$ ). We show the critical range and capacity at which the transition occurs.

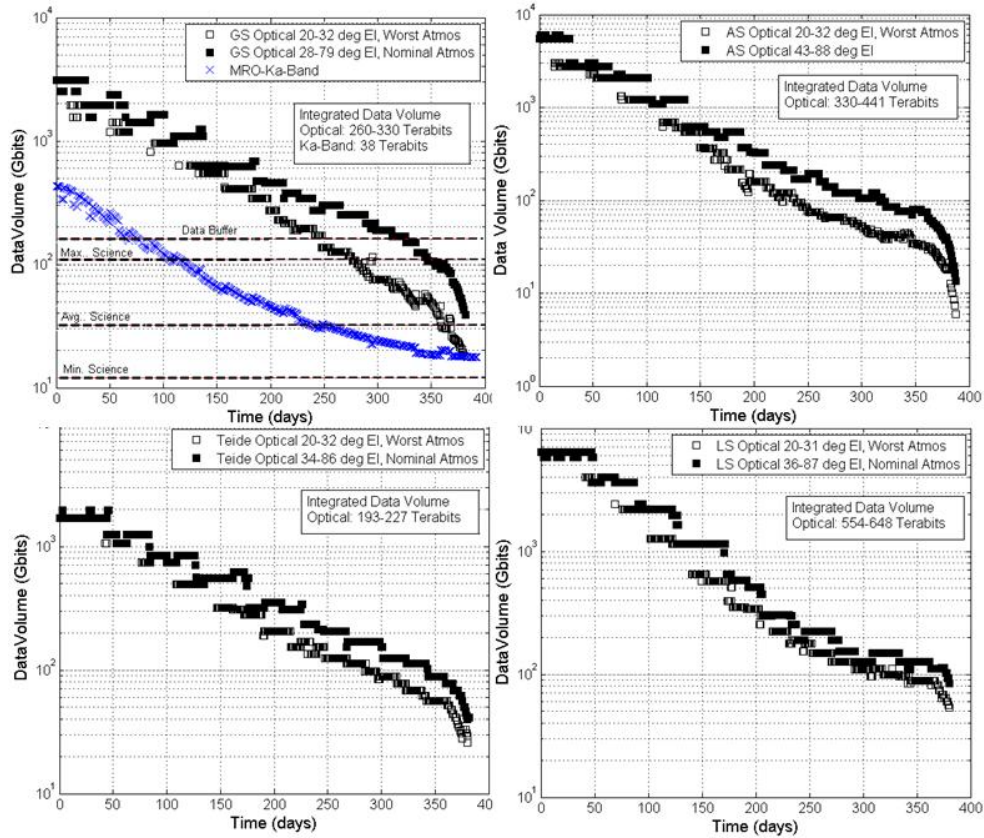


Figure 5. Data volume estimates at Goldstone, CA (GS); Alice Springs Australia (AS); Teide, Canary Islands and La Silla, Chile (LS). The epoch corresponds to July 30, 2018 and the duration analyzed is 389 days.

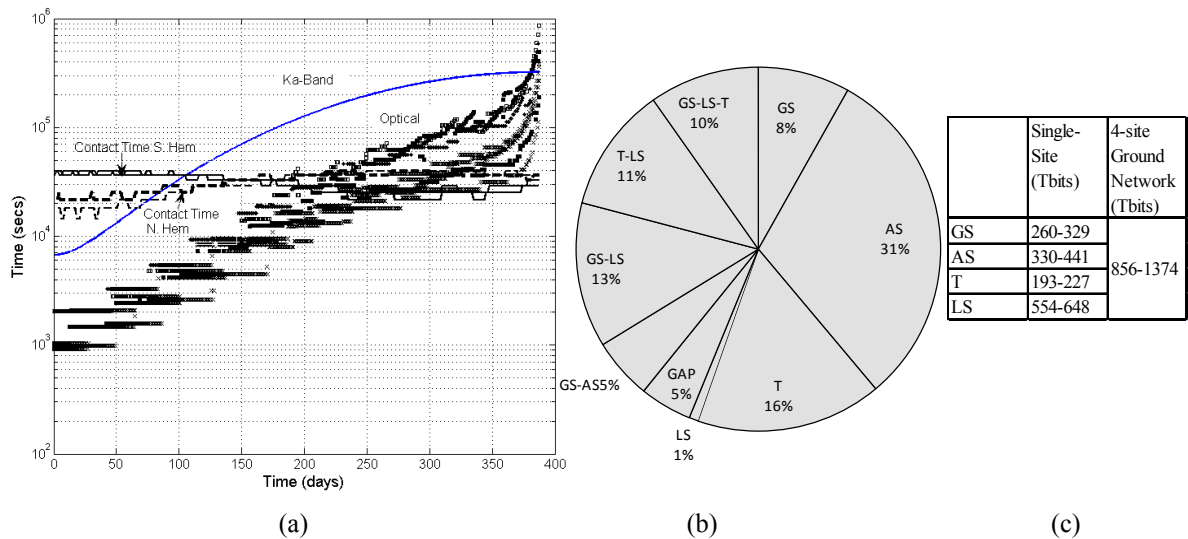


Figure 6. (a) Time to empty the spacecraft buffer optical (points) and Ka-band (line) compared to single-site contact time; (b) increased percentage contact time with ground network comprised of Goldstone (GS), Alice Springs (AS), Teide (T) and La Silla (LS) provides with 5% overall gap (GAP) time. 2-site (GS-AS, GS-LS, T\_LS) and 3-site (GS-LS-TS) with increase availability are also accessible; (c) comparison of integrated data volumes of any single site to all four sites.

Suppose the system is limited primarily by the peak and average power constraints, and not by the bandwidth (here we refer to the available electrical and optical component bandwidth and not the laser carrier bandwidth). The capacity of the peak and average power constrained channel is<sup>10</sup>

$$C = ((P_r + P_n / M) \log_2(1 + MP_r / P_n) - (P_r + P_n) \log_2(1 + P_r / P_n)) / E \quad (1)$$

where C has units of bits/second, M is the peak to average power ratio (for M-ary PPM), and E is the energy per photon, in Joules. To clarify tradeoffs, we utilize the following approximation to the capacity:

$$C \approx C' = \frac{1}{E \ln(2)} \left( \frac{P_r^2}{P_r / \ln(M) + 2P_n / (M-1)} \right) \quad (2)$$

It is straightforward to show that  $C/C' \rightarrow 1$  in the limits as  $P_r \rightarrow 0$  and as  $P_r \rightarrow \infty$ . Moreover C' is a sufficiently good approximation to C for our purposes. We see that at high SNR the capacity goes as  $P_r$ , while at low SNR the capacity goes as  $P_r^2$ . The received signal power may be expanded as

$$P_r = EIRP \left( \frac{D_r}{4R} \right)^2 \eta \quad (3)$$

where, EIRP is the effective isotropically radiated power,  $D_r$  is the receive aperture diameter, R is the range, and  $\eta$  is the overall system efficiency. Suppose the system efficiency is not a function of the range or noise power (This is not, in general, a good assumption, since, for example, the pointing error may increase with the range. Nonetheless, it is sufficient for our immediate purpose, which is to focus on the impact of range loss.)

Substituting the received power into Eqn. 2, we see that  $C \propto 1/R^2$  for  $SNR \gg 2 \ln(M)/M$  and  $C \propto 1/R^4$  for  $SNR \ll 2 \ln(M)/M$ . The transition between the regions occurs where the intensity-modulated direct-detected channel transitions from a self-noise, or shot-noise, limited regime (high SNR) to a background noise limited regime (low SNR). This differs from the coherent microwave channel, which is thermal noise limited, and goes as  $1/R^2$  everywhere. This behavior was also noted<sup>11</sup> for an APD receiver or a receiver using an erbium-doped fiber optical amplifier.

Suppose the noise power is approximated as being proportional to the receive aperture

$$P_n = \alpha \left( \frac{\pi D_r^2}{4} \right)$$

where  $\alpha$  is the noise power spatial density at the receive aperture, in  $W/m^2$ , over a fixed spectral band of interest. This is the case, for example, when the noise is dominated by spatially invariant sky radiance, the diameter is much larger than the atmospheric-coherence-length, so that the receiver field-of-view is fixed, and the system bandwidth and loss are fixed<sup>12</sup>. Then the critical range at which the system switches regimes, where  $P_r/P_n = 2 \ln(M)/M$ , corresponds to the range

$$R^* = \sqrt{\frac{EIRP(M-1)\eta}{8\pi\alpha \ln(M)}}$$

Of course, for a given received signal and noise power, the receive terminal is blind to the range of the receiver. In this respect, from the perspective of the receive terminal, the system has a critical capacity characterizing the switch from the high to low SNR regime. That is, for a given received noise power  $P_n$ , and PPM order M, if the system is required to support a certain data rate, it is necessarily either in the high or low SNR regime, regardless of the range. This critical capacity is approximated by

$$C^* = P_n \left( \frac{(\ln(M))^2}{E \ln(2)(M-1)} \right)$$

Figure 7 illustrates these concepts for the example with the tabulated parameters on the right of the plot. The capacity  $C$ , and its approximation  $C'$  are plotted versus Mars range with the critical range and critical capacity of the transition. In this case the critical rate, or capacity is at 4.7 Mbps, and the critical range is at 2.4 AU. Hence, for the transmit terminal, receiver aperture, and noise power defined the capacity goes as  $1/R^4$  at ranges beyond 2.4 AU. Similarly, for the noise power and PPM order for any link supporting a capacity in excess of 4.7 Mbps, the capacity is going as  $1/R^2$ .

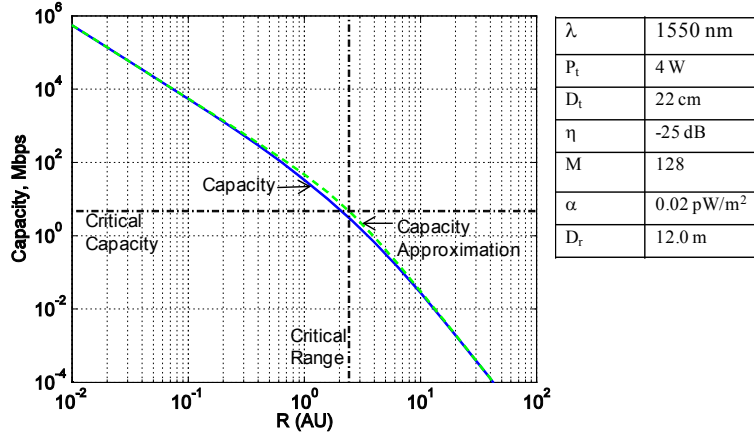


Figure 7. The achievable capacity as a function of the range for the link parameters tabulated on the right of the plot displays the critical range and critical capacity for both the capacity and its approximation.

## 2.6 Enabling Technologies

Critical technologies needed to meet the data-volume estimates presented above are briefly enumerated in this section. Laser transmitter peak-to-average power ratios of  $\sim 160$  for the laser transmitter<sup>13</sup> have been presumed. A pointing control scheme that has been partially validated through simulation<sup>14</sup> and is being developed in the laboratory<sup>15</sup> was also assumed. The ground receiver presumes 12m diameter collecting apertures<sup>6</sup> which also require large, efficient, photon-counting arrays<sup>16</sup> sensitive to 1550 nm photons. As mentioned earlier the architecture assumes Earth transmitted beacon lasers to assist acquisition and tracking. It has been shown that ground laser transmitter powers<sup>4</sup> as high as 5 kW with space-qualified photon counting arrays<sup>5</sup> on the flight terminal would also be required. Efforts to advance these technologies are underway and the cited references in this section point at some of the developments underway in this direction.

## 3. OUTER PLANET MISSIONS

### 3.1. Reference Missions

Applying optical communications to outer planetary missions would introduce the challenges of larger distances. A concern has been the ability to deliver the needed beacon irradiance for assisting acquisition and tracking. Analysis based on the DOT conceptual design, extended to the outer planet ranges of Jupiter and Saturn is discussed in Section 3.2 below. The durations at small sun angles would also be a concern for these missions and were studied for Jupiter.

The Jupiter Europa Orbiter (JEO) mission concept was used for reference. This mission concept includes a Jovian tour followed by a Europa orbit phase<sup>17</sup> with the latter phase driving the downlink data rate requirement. At a maximum range of 6.5AU the baseline JEO design would provide a downlink data rate requirement of 134 kbps, with a Ka-Band system. For the purpose of this study we investigate the viability of achieving a factor of 10 higher data rate, or about 1.5 Mbps at 6.5 AU.

The JEO mission concept would also add the challenge of designing for a high radiation environment. We do not address the radiation issue specifically for an optical system in this paper.

### 3.2. Laser Beacon for Outer Planet Missions

The DOT concept design beacon used served two functions, namely, as a pointing reference for assisting acquisition tracking from space and for a high-rate (~ 300 kb/s max) uplink. We address only the first of these functions for Jupiter and Saturn. Mean beacon irradiance must be delivered to the flight terminal aperture, to satisfy a specified signal-to-noise on the focal plane array with single photon-counting sensitivity at 1030 nm. As the spacecraft moves to farther distances beyond Mars the background contributed from Earth upwelling radiance, as well as, stray solar light actually would start decreasing so that the Earth transmitted laser power to maintain the specified irradiance does not increase proportionately to the inverse square distance. This assertion is supported by analysis. These initial analysis results are summarized with the sparse table presented in Table 3 below. The flight terminal aperture diameter was scaled up to 40 cm and the ground transmitted power in kW is shown for representative range, SEP and SPE from Jupiter and Saturn.

Table 3 Ground laser power in kW needed to deliver the irradiance for acquisition /tracking with 40 cm diameter aperture terminal from indicated range and sun-angle at Jupiter and Saturn

		SEP (deg)																					
		174	163	122	107	91	61	32	29	20	17	8											
Range (AU)	4.5	4																					
	5.5												6										
	6.4																					9	
	9.2				7																		
	9.7					8																	
	10.2										7												
	10.7																						9
	11.0																						10
		1	3	5	6	10	5	3	5	2	1	2											
		SPE Angle (deg)																					

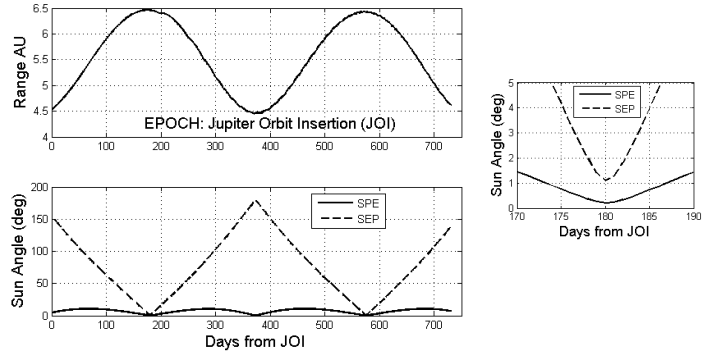


Figure 8. Mission profile, showing range and sun angles encountered for Europa orbiter following orbit insertion. Inset on right shows expanded time scale.

### 3.3. Downlink

The Jupiter reference mission presents operating points represented by the range and sun-angles plotted in Figure 8. The inset on the right of Figure 8 shows an expanded time and Sun angle scale during solar conjunction. If the 12 m ground collecting telescope cannot operate closer than 5-degrees from the Sun an outage of 12-15 days occurs approximately once a year. As mentioned in section 3.2 we evaluate link performance with similar DOT system link characteristics except for scaling the flight terminal aperture diameter from 22 cm to 40 cm. Figure 9 summarizes the expected performance bounded for worst and nominal atmospheric conditions at GS.

The reader is reminded that the link assumes a 12m ground collecting aperture with a 50% detection efficiency photon-counting receiver at its focal plane. PPM-128 with a 0.66 rate serially concatenated code is also assumed. The data-rate exhibits a steeper rate of decrease than the inverse square distance (gray lines).

The Ka-band data-rate is shown with a dashed-dotted line in Figure 9. An approximate estimate of data-volumes assuming 90% availability of the Ka-band and 66% average availability of the optical link indicates 2.5 – 9.1 Tbits per year compared to 0.6 Tbits for Ka-band. All the effects that were shown for the Mars reference mission in terms of increased contact time and availability of the optical link with a ground network would apply to the Jupiter reference mission as well.

Note that the performance shown for the Europa reference mission has been constrained by the enabling technologies that were called out in Section 2.4. Scaling of the flight terminal aperture has been presumed and this would result in an approximate 3 times increase in the mass of the flight optical assembly. The scaling would also require nearly twice as good pointing control because of the narrower beam.

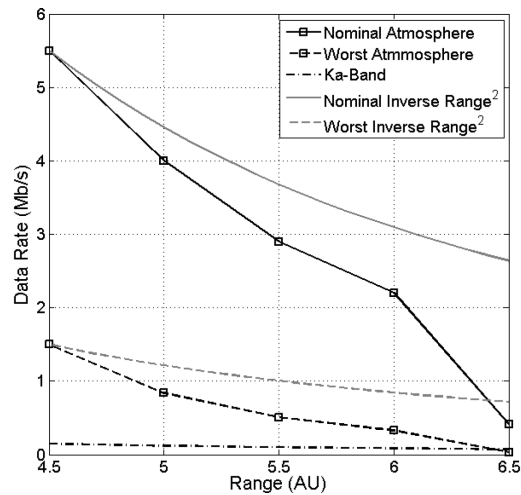


Figure 9. Instantaneous data-rates that could be supported with a 12m diameter ground collector equipped with photon-counting receiver with signaling at PPM 128 and serially concatenated PPM code with 0.66 rate.

## 4. SUN-EARTH LAGRANGE POINT MISSIONS

### 4.1 Astrophysics and Heliophysics Missions

The Lagrange points L2 and L1 on the “night” and Sunlit side of Earth where gravitational and orbital motion forces balance each other, are favored for heliophysics (L1) and astrophysics (L2) missions.

An objective for NASA’s Astrophysics Program is to understand the physics of star formation and galaxy formation. The decadal report for astrophysics (Astro 2010) recommends a 4 m visible/UV observatory to address this, and other objectives. The proposed required sensitivity, resolution and coverage yields a driving case for future downlink data rate requirements. A mission concept study called the Telescope for Habitable Exoplanets and Interstellar/Intergalactic Astronomy<sup>18</sup> (THEIA) is consistent with this recommendation and serves here as the reference mission for astrophysics.

The proposed THEIA Observatory would operate at Earth-Sun L2 (in halo orbit similar to JWST) and among other instruments would consist of a Star Formation Camera (SFC) instrument. The SFC would produce, by far, the largest data volume and *establish* the maximum downlink data rate requirement for astrophysics missions. Detailed design reference mission studies project a maximum daily data volume of 6 TBytes associated with conducting deep cosmological surveys over relatively wide fields.

The Solar Dynamics Observatory<sup>19</sup> (SDO), in operation in geosynchronous orbit, uses the highest downlink data rate of any heliophysics mission to date. SDO nominally downlinks a continuous data stream to a dedicated 12 m station in New Mexico at Ka-Band at a rate of 150 Mbps. The SDO design represents a compromise between spatial, spectral and temporal resolution, as constrained by the capabilities of currently available telecommunications systems. Science performance would benefit from better resolution. Therefore, for the purpose of this study, we hypothesize a SDO follow-on mission with 10× downlink data rate (1.5 Gbps) and operating at Earth-Sun L1 (between Sun and Earth). We assume use of the same orbit as the Solar and Heliospheric Observatory<sup>20</sup> (SOHO) spacecraft.

### 4.2 Optical Communication Link Parameters

Figure 10 shows the elevation angles experienced from Table Mountain, CA and La Silla, Chile in order to contact the proposed THEIA and SOHO mission spacecrafts at Sun-Earth Lagrange (L2 and L1 respectively) points. For the proposed THEIA Mission an outage would be experienced with either a northern or southern hemisphere site indicated by the days when the elevation angles are less than 20-degrees. However, the sites complement each other so that a combination of ground sites in both hemispheres would not only increase contact time by eliminating outages but would

also increase availability because of overlap in coverage. Even though an outage is not observed for the SOHO mission, significantly reduced contact times are avoided by having coverage from northern and southern hemispheres. Similar coverage and availability effects as pointed out for the Mars reference mission are expected for these Lagrange reference missions and the detailed analysis to quantify these effects was not carried out.

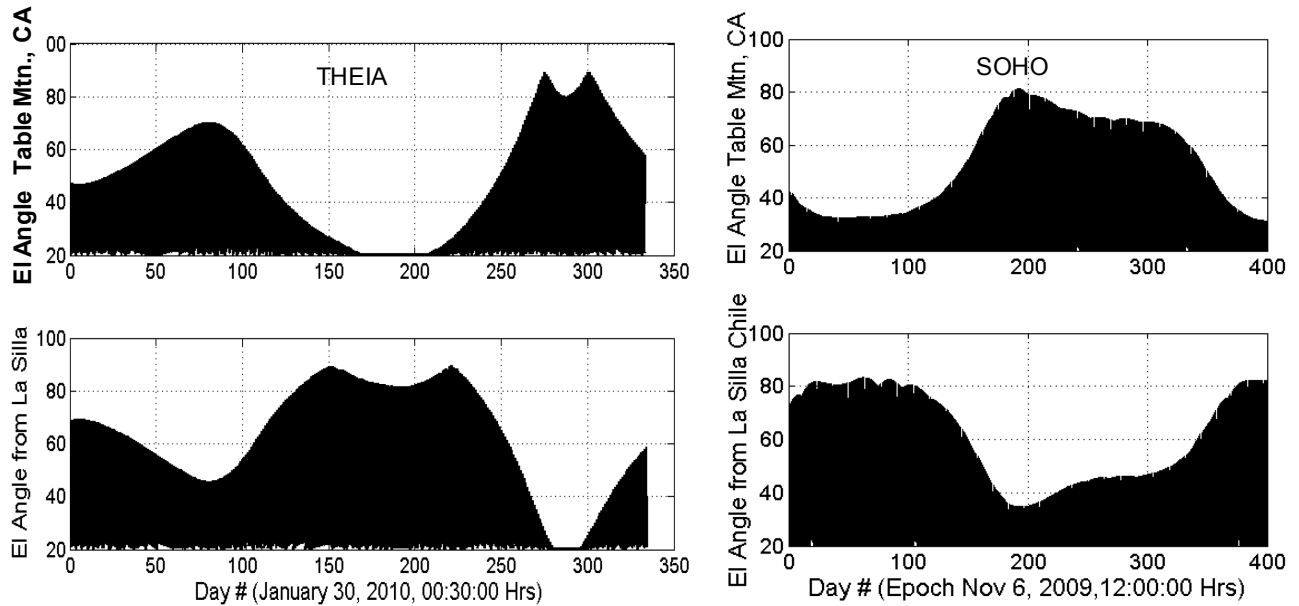


Figure 10. Coverage from northern (Table Mountain, CA) and southern (La Silla, Chile) ground sites for a Sun-Earth L2 reference mission like the THEIA concept and a Sun-Earth L1 reference mission such as SOHO provide complimentary coverage.

Figure 11 shows the range and sun-angles encountered for the L2 and L1 reference missions. While the ranges would be comparable, the SEP angle for L2 reference missions would be large so that, for the entire mission, the ground site would be contacting the spacecraft with night sky additive background noise. On the other hand for L1 reference missions the SEP angles would be small ranging from approximately 5-20 degrees so that optical communications for L1 reference missions would be degraded by additive background from sky radiance and stray light. The space terminal in the case of L2 reference missions would be continuously subjected to low SPE angles ranging from 25-40° whereas for L1 reference missions the space-terminal would always be looking at sunlit Earth.

### 4.3 Link Performance

The link performance for the Lagrange reference missions was evaluated using a flight terminal identical to that used for the DOT study i.e., 22 cm aperture diameter with 4 W average laser power and corresponding signaling. For the ground receiver, because the range would be significantly reduced compared to planetary distances, a 1-m diameter ground collecting aperture with photon-counting receivers was assumed. By reducing the aperture diameter the size of the photon-counting arrays would be relaxed.

For the L2 reference mission we project a data-rate of 750 Mb/s with 4.7 dB link margin and 175 ps slot widths. Atmospheric transmission @1550 nm of 0.9 and turbulence represented by  $r_0 = 3\text{cm}$  @ zenith @ 500 nm, were assumed, representing > 90<sup>th</sup> percentile for Table Mountain, CA.

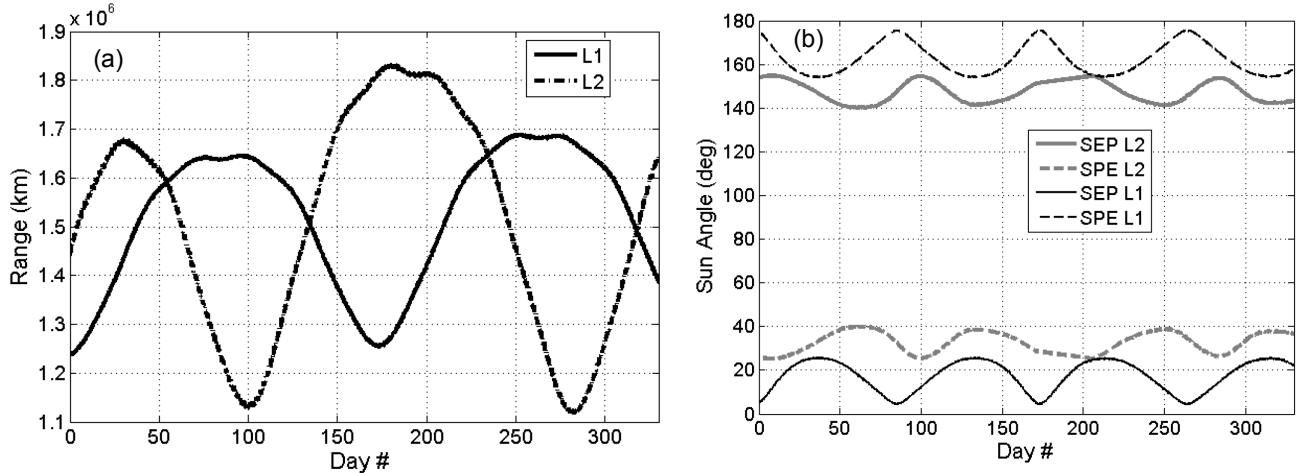


Figure 11. (a) Range for sun-Earth L1 and L2 reference missions; (b) SEP and SPE angle for L2 and L1 reference missions.

For the L1 reference mission the maximum range shown in Fig. 11 with a sky radiance of  $1.2E-2 \text{ W/cm}^2/\text{sr}/\mu\text{m}$  was used along with the same atmospheric transmission and turbulence as the L2 reference mission. A data-rate of 650 Mb/s with a range of 3-dB was estimated using slot-widths of 200 ps.

Data-rates reported for L2 and L1 above are lower bounds, since worst atmospheric conditions with maximum range were presumed. Combining the pie distribution shown in Fig. 6b, with the availability shown in Table 2 would result in 95% contact time or 15 hours of downlink per day. In order to downlink 6 TBytes of data a data-rate of  $\sim 900 \text{ Mb/s}$  would be required which is larger than the 650-750 Mb/s derived above. What we propose is at least two wavelength-division multiplexed (WDM) channels each operating at 650-750 Mb/s as indicated above. Thus instantaneous downlink data-rates of 1.3-1.5 Gb/s could be achieved. With this data rate the 6TB of data volume per day could be transferred with sufficient margin.

The proposed strategy to meet the data-volume target will need incremental development of narrower slot widths compared to the DOT concept design. Furthermore because the distances are considerably shorter than planetary ranges requirements on ground collecting aperture diameter, photon-counting array size, Earth transmitted beacon laser power and flight terminal acquisition/tracking detector could be relaxed.

Note that we have identified a solution for achieving the data-volumes called for by potential future astrophysics and heliophysics missions. There is considerable trade space, like choosing larger ground aperture diameters and trading it either for flight terminal resources or choosing wider slot-widths for ease of implementation.

## 5. CONCLUSIONS

In this paper future deep-space mission concepts of interest were examined in order to assess whether a  $10\times$  increase in data-volume return could be achieved relative to state-of-the-art radio frequency telecommunication systems. For the missions considered under conservative assumptions this could be achieved provided the indicated technology development advances and matures. Short mission durations when shallow sun-angles effect rather severe signal-to-noise degradation and corresponding downlink capacity were pointed out. These link conditions and the corresponding observed worse than inverse-square dependence of deep-space optical links deserves further study.

## ACKNOWLEDGEMENTS

This work described was carried out at the Jet Propulsion Laboratory (JPL), California Institute of Technology under contract with the National Aeronautics and Space Administration (NASA).

## REFERENCES

- [1] Hamid Hemmati, Abhijit Biswas and Ivan B. Djordjevic, "Deep-Space Optical Communications: Future Perspectives and Applications," Proceedings of the IEEE, 99, 2020-2039, 2011.
- [2] Shiro Yamakawa, Tasuyuki Hanada and Hiroki Kohata, "R&D Status of the Next Generation Optical Communication Terminals in JAXA," 2011 International Conference on Space Optical Systems and Applications, 391-395.
- [3] Don M. Boroson, Bryan S. Robinson, Dennis A. Burianek, Daniel V. Murphy, "Overview and status of Lunar Laser Communications Demonstration," Proc. SPIE, 8246, 2012.
- [4] Abhijit Biswas, Hamid Hemmati, Sabino Piazzolla, Bruce Moision, Kevin Birnbaum, and Kevin Quirk, [http://tmo.jpl.nasa.gov/progress\\_report/42-183/title.htm](http://tmo.jpl.nasa.gov/progress_report/42-183/title.htm).
- [5] William Farr, Martin Regehr, Malcolm Wright, Doug Sheldon, Adit Sahasrabudhe, Jonathan Gin and Dan Nguyen, "Overview and Design of the DOT Flight Laser Transceiver," [http://tmo.jpl.nasa.gov/progress\\_report/42-185/title.htm](http://tmo.jpl.nasa.gov/progress_report/42-185/title.htm).
- [6] Kevin Birnbaum, Jeffrey R. Charles, William H. Farr, Jonathan Gin, Kevin J. Quirk, William T. Roberts, Jeffrey A. Stern and dYen-Huang Wu, "DOT Ground Laser Receiver Overview and Major Trades," [http://tmo.jpl.nasa.gov/progress\\_report/42-182/title.htm](http://tmo.jpl.nasa.gov/progress_report/42-182/title.htm).
- [7] W. Thomas Roberts and Malcolm Wright, "Deep-Space Optical Terminals (DOT) Ground Laser Transmitter (GLT) Trades and Conceptual Point Design," [http://tmo.jpl.nasa.gov/progress\\_report/42-183/title.htm](http://tmo.jpl.nasa.gov/progress_report/42-183/title.htm)
- [8] S. Piazzolla, J. P. Wu, M. Franco, D. Hoppe, "Preliminary assessment of the atmospheric channel at Goldstone, CA," 2011 International Conference on Space Optical Systems and Applications, 220-229.
- [9] "Cloud Free Line of Sight (CFLOS) Study," Subcontract No. 1265502, conducted by TASC Inc., 55 Walkers Brook Drive Reading, MA 01867-3297, under contract to JPL, California Institute of Technology, 2005.
- [10] A. D. Wyner, "Capacity and error exponent for the direct detected photon channel—Part I," IEEE Transactions on Information Theory, vol. 34, Nov. 1988.
- [11] M. Toyoshima, W. R. Leeb, H. Kunimori, and T. Takano, "Comparison of microwave and light wave communication systems in space applications," Optical Engineering, vol. 46, # 1, 2007.
- [12] S. Piazzolla, in Chapter titled "Atmospheric Channel," of Near-Earth Laser Communications, [Ed. H. Hemmati] CRC Press, 2009
- [13] Malcolm W. Wright, "Preliminary results of space grade laser transmitters for optical communications," Proc. SPIE, 8246, 2012
- [14] Joel F. Shields, Martin Regehr, Abhijit Biswas, "Simulation of deep space optical transceiver," Proc. SPIE, 8246, 2012.
- [15] Gerardo Ortiz, Virginio Sannibale, "Low-frequency vibration isolation system for deep space optical communications payload," Proc. SPIE, 8246, 2012.
- [16] Wiliam H. Farr, Jeffrey Stern, "Superconducting nanowire arrays for multi-meter free space communications," Proc. SPIE, 8246, 2012.
- [17] <http://opfm.jpl.nasa.gov/europajupitersystemmissioneism/>
- [18] <http://www.astro.princeton.edu/~dns/Theia/teamX.pdf>
- [19] <http://sdo.gsfc.nasa.gov/>
- [20] <http://sohowww.nascom.nasa.gov/>